Hydrogeology Journal (2019) 27:2137–2154
https://doi.org/10.1007/s10040-019-01982-5

REPORT

Hydrogeology of an alpine talus aquifer: Cordillera Blanca, Peru

Robin Glas[1] · Laura Lautz[1] · Jeffrey McKenzie[2] · Robert Moucha[1] · Daniel Chavez[2] · Bryan Mark[3] · John W. Lane Jr[4]

Received: 13 August 2018 / Accepted: 1 May 2019 / Published online: 21 May 2019

Abstract

The dramatic loss of glacial mass in low latitudes is causing shifts in downstream water availability and use during the driest months of the year. The world's largest concentration of tropical glaciers lies in the Cordillera Blanca range of Peru, where glacial runoff is declining and regional stresses are emerging over water resources. Throughout the Cordillera Blanca, groundwater inputs from alpine meadow–talus complexes, locally known as pampas, supply proglacial streams with up to 80% of their flow during the region's dry season. Structural knowledge of the pampa aquifers is needed to estimate their drainable groundwater storage capacity and residence time, to elucidate the role and importance of alpine groundwater storage in the regional water budget of the Cordillera Blanca. To understand the structure of these proglacial aquifers, multiple near-surface geophysical methods were implemented in a proglacial valley near dense networks of spring-fed tributaries. Geophysical results and borehole logs suggest groundwater is stored in a confined aquifer composed of buried talus deposits overlain by lacustrine clay, while deeper portions of the unit, 10–15 m in depth, are relatively clay-free and more hydraulically conductive. Based on these findings and assumptions of aquifer porosity, the pampas of the Callejon de Huaylas may store from 0.006 to 0.02 km^3 of groundwater. Furthermore, these findings suggest that the talus aquifers of the Cordillera Blanca were formed in proglacial lakes, followed by infilling with fine lacustrine sediments that confine lower units and allow for groundwater discharge to springs via macropores and preferential flow.

Keywords Alpine groundwater · Peru · Geophysical methods · Climate change · Cordillera Blanca

Introduction

In the tropics, mountain glaciers are especially sensitive indicators of climate change, with ice loss accelerating in the presence of warming regional temperatures (Burns and Nolin 2014; Kaser and Osmaston 2002; Vuille et al. 2008).

Electronic supplementary material The online version of this article (https://doi.org/10.1007/s10040-019-01982-5) contains supplementary material, which is available to authorized users.

✉ Robin Glas
robin.glas@gmail.com

1 Department of Earth Sciences, Syracuse University, 204 Heroy Geology Laboratory, Syracuse, NY 13244, USA

2 Department of Earth and Planetary Sciences, McGill University, 3450 University Street, Montréal, QC H3A 0E8, Canada

3 Department of Geography, The Ohio State University, 1136 Derby Hall, 154 North Oval Mall, Columbus, OH 43210, USA

4 Earth System Processes Division, U.S. Geological Survey, Hydrogeophysics Branch, 11 Sherman Place, Unit 12 5015, Storrs, CT 06269, USA

Average annual warming in tropical zones around the globe is projected to surpass 4 °C by the year 2100 at elevations higher than 4,000 m above sea level (masl) using the higher emissions scenario A2 (Nakicenovic et al. 2000), which would result in a significant regional decline in ice mass (Bradley et al. 2006; Vuille et al. 2018). Historically, there have been no clear annual precipitation trends in the Cordillera Blanca (northwestern Peru) since 1970 (Racoviteanu et al. 2008), although a positive shift toward higher precipitation amounts was observed in the mid-1990s during the region's wet season (December–February; Schauwecker et al. 2014). Projections of precipitation amounts into the twenty-first century for the tropical Andes are also highly uncertain according to regional climate models and varying emissions scenarios, with low spatial coherence between climate models and both regions of slightly increasing and decreasing amounts (Urrutia and Vuille 2009).

More than 99% of glaciated area in the tropics lies in the Andes Mountains, which divide the inner (continuous annual precipitation) from outer (seasonal precipitation) tropical zones (Kaser 1999). Many glacially fed rivers and streams that drain the western side of the Cordillera Blanca have already surpassed the temporary increase in flow caused by glacial retreat, and have begun to recede toward dry season streamflow that is more closely coupled to seasonal precipitation patterns (Baraer et al. 2012; Chevallier et al. 2011). This glacial retreat is accelerating, indicating that these reductions in dry season streamflow will reflect declining contributions from glacial melt into the twenty-first century (Bury et al. 2013; Huss et al. 2017). Compared with the mid to higher latitudes, the tropics have been relatively understudied in terms of hydrologic processes that contribute to regional water resources.

The Cordillera Blanca contains a quarter of the world's tropical glaciers, which are an important source of meltwater for a variety of downstream uses (Chevallier et al. 2011; Racoviteanu et al. 2008). A large portion of glacierized area of the Cordillera Blanca drains westward to the Santa River, which flows toward the northwest and eventually to the Pacific Ocean (Mark et al. 2005). The Santa River is the primary dry season water source for vast agricultural and industrial operations in the region, as well as hydroelectric power generation for approximately 10% of the country (Bury et al. 2013). Dry season flow rates in the Santa River watershed are projected to further decline with the retreat and relative loss of glacial meltwater as a source of flow to the river's headwater streams (Juen et al. 2007). Regional warming in the Cordillera Blanca is driving the region's loss of glaciers (Schauwecker et al. 2014), with increasing temperature trends of 0.13 °C/decade since the 1950s recorded for the tropical Andes (Vuille et al. 2015). As the glaciers retreat at accelerating rates (Burns and Nolin 2014), groundwater that is recharged by precipitation will increasingly be a dominant source of flow during the dry season (Baraer et al. 2015), although the hydrogeology of these alpine systems is not yet fully understood.

During the dry months of May–October, a combination of glacial meltwater and alpine groundwater supplies the majority of streamflow in the Callejon de Huaylas basin (Mark et al. 2010). Although the glacial melt contribution to dry season streamflow for the Santa River is well documented as proportional to the glacial coverage in four groundwater study catchments, (Baraer et al. 2009, 2012, 2015; Glas et al. 2018; Mark and Mckenzie 2007; Mark et al. 2005; Pouyaud et al. 2005), the groundwater system that supplies the region's alpine tributaries is not well understood (Baraer et al. 2009, 2015; Chavez 2013; Gordon et al. 2015; Maharaj 2011; Somers et al. 2016). Studies of groundwater hydrology in the Cordillera Blanca have reported a significant contribution of groundwater to proglacial streams during the dry season, and have inferred the aquifer structure of headwater valley aquifers based on groundwater chemistry and borehole logs from shallow wells (Chavez 2013; Gordon et al. 2015). To predict the role of groundwater in sustaining streamflow during future dry seasons, estimates of drainable groundwater storage and residence time distributions are required. Such estimates require geologic structural knowledge of the proglacial sediments and talus deposits that are hypothesized to serve as the region's headwater aquifers.

Worldwide, glaciated alpine catchments contain slope deposits such as talus cones, debris fans, and moraines that are important permeable geomorphic features for storing groundwater and providing stream baseflow. Despite their importance, these features are understudied in the tropics, where glacial valley sediments contain less permafrost and snowpack than temperate and arctic regions (Haeberli et al. 2010). Studies of the structure and aquifer function of slope deposits are generally restricted to the mid-latitudes of the Northern Hemisphere, where talus slopes, moraines, and debris fans are shown to recharge with precipitation and/or snowmelt, and delay discharge to proglacial valley streams (e.g. Clow et al. 2003; McClymont et al. 2010). Proglacial fluvial sediments have been shown to be important for groundwater storage in temperate alpine zones (e.g. Pourrier et al. 2014), while low-permeability basal till promotes resistance to flow and groundwater retention (e.g. Winkler et al. 2016). In both the Canadian Rockies (Muir et al. 2011) and the Bolivian Andes (Caballero et al. 2002), talus deposits have relatively short water residence times (event-scale or 24–28 h) and high hydraulic conductivity (0.01–0.03 m s^{-1}). In the valleys of the Cordillera Blanca, fine-grained silts and clay deposits play an important hydrogeologic role in talus groundwater transmission, although the nature of this role is poorly understood.

Alpine slope deposits such as talus and debris fans have been conceptualized as major components of the groundwater system of the Cordillera Blanca, but more information about the subsurface is needed to determine the depth of any confining layers and overall aquifer thickness. Previous studies using hydrochemistry, ground penetrating radar, borehole data, and dilution tracing experiments support the hypothesis that permeable talus deposits exposed at the lateral edges of proglacial headwater valleys are likely areas of aquifer recharge (Baraer et al. 2015; Chavez 2013; Gordon et al. 2015; Maharaj 2011). These investigations also suggest that buried talus supports the primary aquifer in proglacial valleys of the Cordillera Blanca, where talus layers are confined by lacustrine sediments at the surface and transit time is long enough to sustain dry season flow. Better constraints on the sediment composition of these talus aquifers are needed to determine their storage capacity, as well as average groundwater residence time and rate of turnover.

Near-surface geophysical methods are useful when studying the hydrogeology of remote alpine catchments where scant hydrologic data exist and deeper boreholes and road access are not feasible. To test the current conceptual models of groundwater recharge and discharge, this study provides a structural classification (sediment type, depositional order, inferences about porosity and permeability) of an aquifer in a central valley of the Cordillera Blanca by using multiple near-surface geophysical methods integrated with previous borehole data. This study integrates results from both seismic (refraction and passive seismic) and electrical (1D and 2D resistivity) geophysical methods with observations of geomorphology and hydrology to conceptualize changes in sediment and soil matrix with depth. This integrated approach results in a refined conceptual model of the geomorphic evolution of glaciated valleys of the Cordillera Blanca, and of the sequential sediment deposition that created confined aquifers in headwater valleys that support groundwater storage and discharge to tributaries of the Santa River during the dry season.

Site description

The Cordillera Blanca lies between 8.5 and 10 S latitude and is Peru's highest mountain range (Kaser and Georges 1999). During the dry season, sources of discharge to the Santa River include runoff and groundwater from the nonglaciated Cordillera Negra, which lies to the west, and glacial runoff with groundwater inputs from the Cordillera Blanca on the eastern side of the basin (Mark et al. 2005). The upper portion of the Santa River watershed, known as the Callejon de Huaylas, contains the Cordillera Blanca and has a spatial extent of 4,900 km^2. Within the Callejon de Huaylas, most of the glaciated peaks and corresponding watersheds lie within the boundary of Huascaran National Park (Fig. 1).

The bedrock composition of the Cordillera Blanca consists of the Chicama Formation, a metasedimentary unit dominated by Jurassic Phyllites, which was intruded by a Neogene granodiorite batholith in the late Miocene (Giovanni et al. 2010). Valleys in the southern Cordillera Blanca reveal more exposed Chicama bedrock, and as a result tend to be wider and more expansive than the valleys to the north, which are predominately underlain by granodiorite. Northern and central valleys in the Cordillera Blanca have high, steep granitic bedrock walls and relatively narrow valley widths, with large proportions of glaciated catchment area (Baraer et al. 2015).

Alpine valley catchments in the Cordillera Blanca are dominated by exposed granitic and Chicama in their upper portions, the valley bottoms are carved through Quaternary deposits that form alpine wet meadows (locally called "pampas") that occur as wetlands and grasslands (Giovanni et al. 2010). The valleys are heavily grazed by livestock and are largely saturated throughout the wet and dry seasons (Polk 2016). These low-gradient meadows contain talus slopes and that line the valley walls, providing likely flow paths for wet season-derived precipitation to recharge underlying aquifers, according to hydrochemical evidence in surface water samples (Baraer et al. 2015).

Throughout the alpine valleys of the Cordillera Blanca, the wet meadows are punctuated by cross-valley end moraines and landslide debris deposits. These landslides and moraines once dammed glacial meltwater lakes that have since filled in with fine-grained sediments (Rodbell and Seltzer 2000) and organic soils (Polk 2016) to form the low-gradient wet meadows of the Cordillera Blanca (Mark and Mckenzie 2007). The last glacial maximum in this area was likely between 21 and 34 ka, with rapid glacial retreat underway by 16 ka (Farber et al. 2005). These lakes infilled with clays, silts, and sands beginning 12 ka (Glasser et al. 2009) leading to the terrestrialization of the lake environments. In the wetland-dominated pampas, the lake sediments are overlain by a thin (<0.2 m) layer of peaty organic soil (Chavez 2013; Maharaj 2011). Networks of perennial and ephemeral springs emanate from the toes of lateral talus and debris deposits, as well as from mid-valley points. Spring water forms tributaries that flow into the valley stream and are the primary connection between the streams and the groundwater as evidenced by tracer experiments in the Quilcayhuanca Valley (Gordon et al. 2015; Somers et al. 2016).

Quilcayhuanca hydrogeomorphology

The Quilcayhuanca Valley contains roughly 3.5 km^2 of wet meadow area above 3,800 masl (Baraer et al. 2015; Gordon et al. 2015), and receives meltwater from the Chinchey, Pucaranra, Chopiraju, and Cayesh glaciers. This portion of the Quilcayhuanca Valley consists of two meadows (upper and lower) that are separated by a cross-valley end moraine (Somers et al. 2016). Since the 1930s, two of Quilcayhuanca's four glaciers have reportedly lost considerable ice mass. The Pucaranra glacier lost 690 m of length from 1930 to 1994 (Ames 1998) and the Chinchey glacier lost more than a quarter of its ice-covered area between 1930 and 1970 (Georges 2004). Glacial retreat in the Quilcayhuanca Valley has been linked to a 17.2% reduction in wetland area between 2000 and 2011 (Bury et al. 2013).

This study focuses on the lower Quilcayhuanca meadow that lies just downstream of a cross-valley end moraine, near the Casa de Agua diversion and discharge monitoring station (9.465°S, 77.379°W, 3,905 masl, Fig. 2a). Lateral talus slopes line the Quilcayhuanca Valley and consist of boulders and cobbles (0.2–1 m in diameter) derived from the source rocks of the overlying cliffs, which are primarily granodiorite and metasedimentary (Chavez 2013). At the valley edges, lower portions of the near-vertical (>80°) bedrock valley walls are covered by talus deposits, which form a gentler repose slope of 20–35° (Fig. 2; upper hillslope), then transition to colluvial deposits on lower slopes of 10–20° (Fig. 2; lower hillslope) toward the valley center. The lower colluvial slope intersects with the organic-and clay-rich valley floor, which slopes gently up-valley toward the glaciers at angles less than 10°. The upper and lower hillslopes are covered by loose, dry soils and are

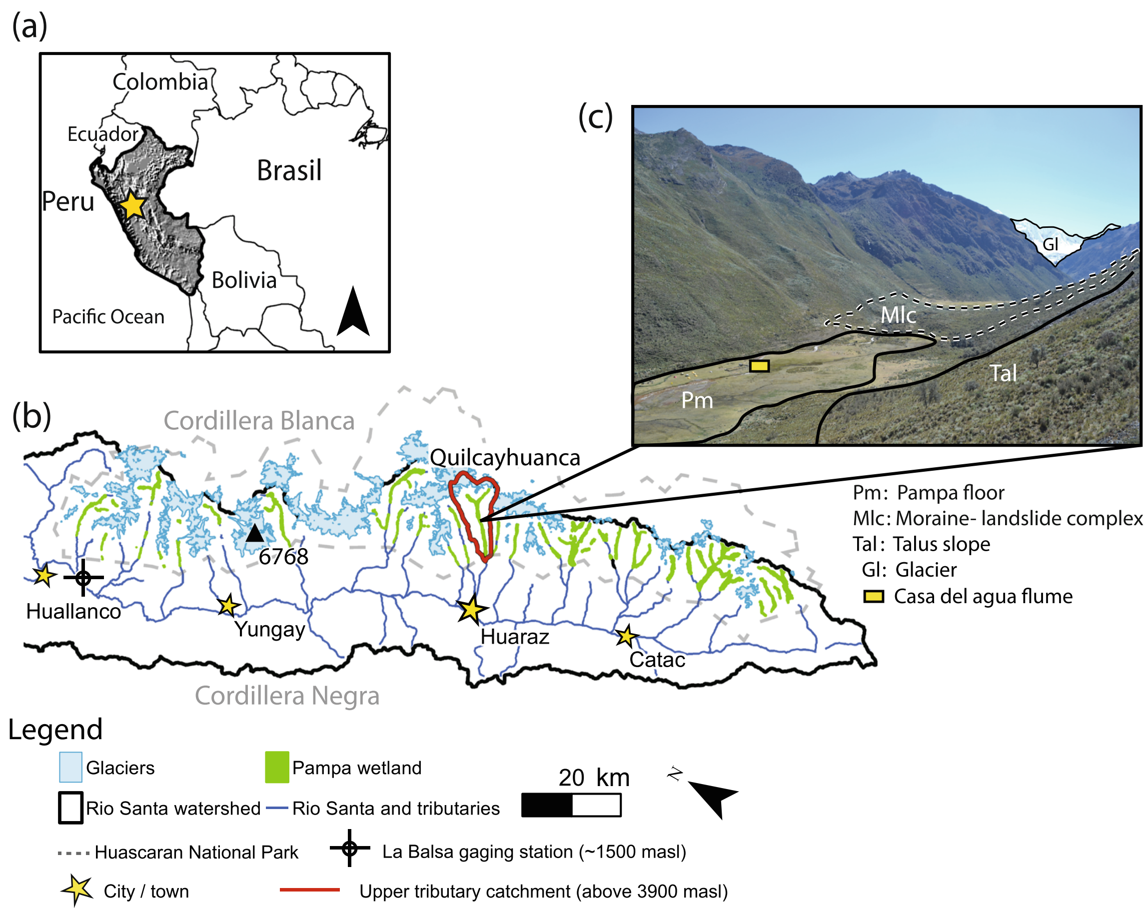

Fig. 1 Study area location. **a** Yellow star marks location of Cordillera Blanca range. **b** Delineation of Callejon de Huaylas basin, which drains to a gaging station at La Balsa via Santa River and tributaries. **c** Photograph (facing north) of Quilcayhuanca Pampa with major geomorphologic features

lightly vegetated with shrubs, grasses, and small alpine trees, whereas portions of the talus deposits higher in elevations are free of soil cover.

Boreholes were drilled by Chavez (2013) in the lower Quilcayhuanca meadow in 2012 and 2013 and completed as seven piezometers (named GW1–GW7) screened in the coarse sediments at the depth of refusal (Fig. 3). According to these borehole logs, the top 2–7 m of sediment consists of lacustrine silty clays and small amounts of fine sand with little to no coarse fragments. At 2–7 m in depth (depth of refusal), boulders were encountered, ranging from 10 cm to 1 m in diameter, accompanied by small amounts of gravel and sand. The boulders are largely composed of granodiorite and andesite, with a small number originating from the metasedimentary Chicama Formation (Chavez 2013).

Hydraulic head in each piezometer generally follows seasonal precipitation patterns, with the lowest groundwater levels around the month of October, marking the end of the dry season (Fig. 3). Artesian pressure was encountered upon drilling piezometer GW2, which had to be permanently sealed to terminate water loss. These pressure conditions suggest that the lower Quilcayhuanca meadow is underlain by a confined aquifer, which transitions to unconfined at the talus slopes near the valley walls (Chavez 2013). During both the wet and dry season, the hydraulic gradient across the piezometer transect (GW7–GW1–GW5–GW6) slopes toward the mid-valley stream, with the highest intra-annual head fluctuations in GW7, the piezometer located closest to the exposed lateral talus deposit.

Previous investigations of surface-water sources in the Cordillera Blanca have shown that isotopic composition varies according to season, proportion of glacial meltwater, and elevation of source precipitation (Mark and Mckenzie 2007; Mark and Seltzer 2003). According to Gordon et al. (2015), in the Quilcayhuanca Valley, water from springs located in the upper and lower meadow were more isotopically enriched than the stream, suggesting that this water did not originate from the glacier. Across these same meadows, the dissolved ion concentrations along with isotopic similarities between several springs indicate that they are sourced from the same aquifer (Baraer et al. 2015). Dye tracing experiments by Somers et al. (2016) suggest that nearly a third of the

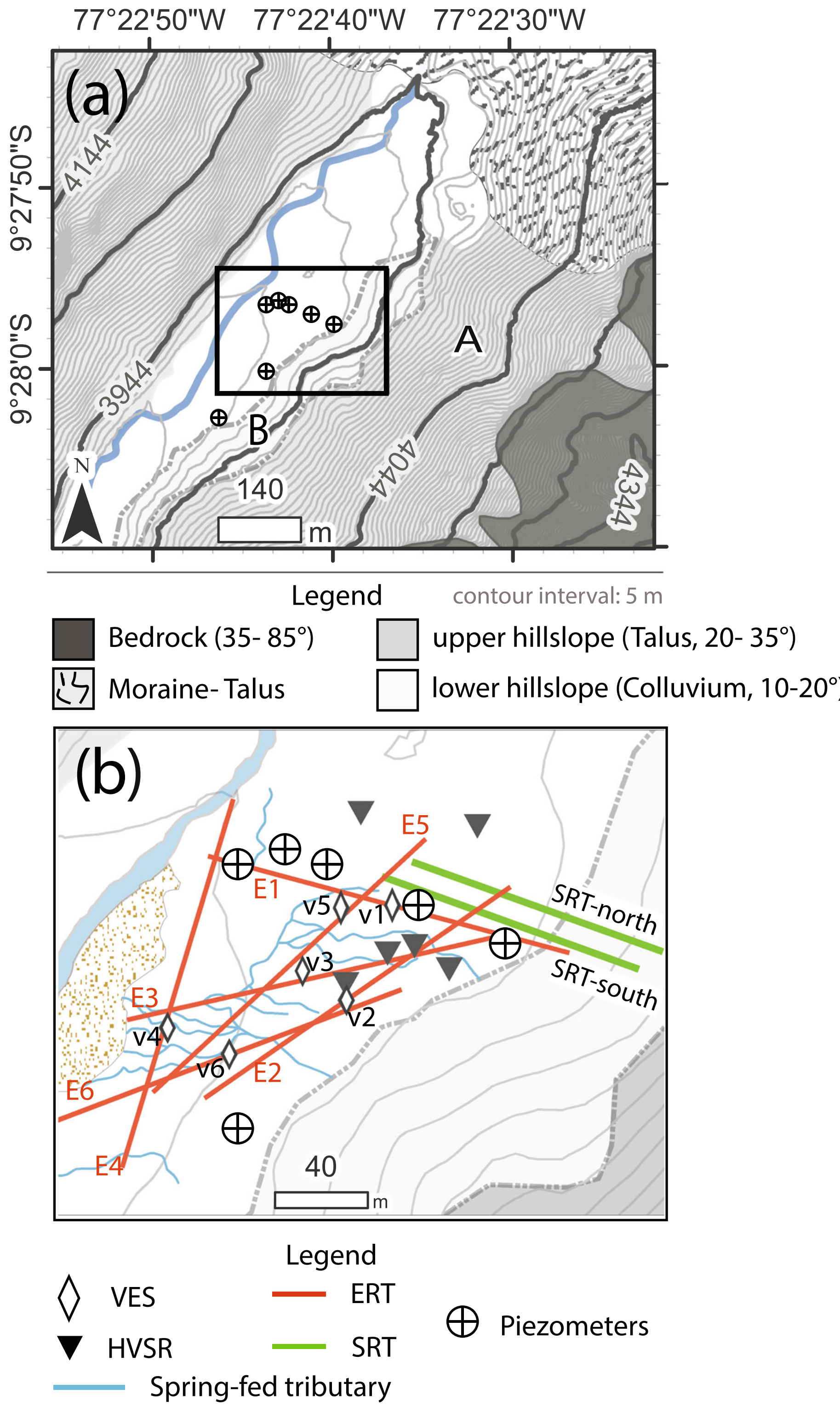

Fig. 2 **a** Study area in Quilacayhuanca lower meadow, including geophysical study area in black box. Dominant topographical slopes indicated by shading. **b** Locations of geophysical transects and soundings, including vertical electrical soundings (VES), horizontal to vertical spectral ratio (HVSR), electrical resistivity tomography (ERT), and seismic refraction tomography (SRT). Locations of spring-fed tributaries delineated by light blue lines

discharge in this approximately 4-km reach was sourced from groundwater that emerges from these valley springs. These recent studies have resulted in a conceptual model where the interaction of slope deposits with lacustrine and glacial sediments creates the conditions for sustained base flow throughout the Cordillera Blanca during the dry season (e.g. Baraer et al. 2015). Although the relative groundwater contribution to the Quilcay stream has been estimated at varying scales (Baraer et al. 2015; Somers et al. 2016), the hydrogeology leading to these types of conditions has only been examined by point measurements made in boreholes.

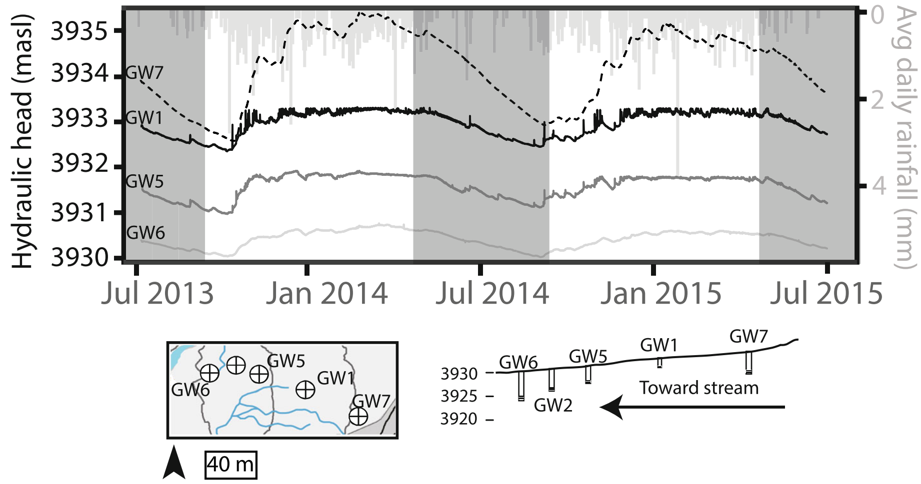

Fig. 3 Time series of hydraulic head levels in piezometer transect GW7–GW1–GW5–GW6, plotted with rainfall hyetograph for reference. Regional dry season from May 1 to Oct 1 shaded in grey. Insets show plan view (left) and profile view (right) of well transect

Methodology

In this study, four types of surface-based geophysical methods were interpreted along with existing well data (drill logs, piezometric head data, groundwater chemistry including major ions and water isotopes) to constrain the extent of buried colluvium, as well as its depth, sediment matrix composition, and depth to bedrock in the Quilcayhuanca Valley pampa. Geoelectrical and seismic methods are complementary and ideal for this study because they respond to differing physical properties of the subsurface and when used in conjunction, can diminish interpretive uncertainty associated with the methods when used in isolation (Cardarelli et al. 2010). In the following, the field and analysis procedures used for each geophysical survey conducted in the austral winters of 2015 and 2016 are outlined.

Seismic refraction tomography

Seismic p-wave velocity is sensitive to hydrogeologic properties such as lithology, porosity, density, and saturation of the subsurface media, where sediments with low porosity and high-saturation propagate p-waves at higher speeds, as do more consolidated and crystalline materials (Haeni 1986). Seismic refraction tomography is a geophysical method widely used to characterize elastic properties of the near-surface in alpine regions (e.g. Langston et al. 2011; Vignoli et al. 2012). Two seismic refraction surveys SRT-south and SRT-north (Fig. 2) were conducted along the piezometer transect spanning the valley floor in July of 2015, targeting the interface between bedrock and unconsolidated valley sediments, as well as changes in sediment composition with depth. Forty-eight vertical component geophones (40 Hz cut-off frequency) were spaced at 2.5 m along two parallel lines SRT-south and SRT-north, for a total length in each survey of 117.5 m. The survey lines spanned the transition between the relatively flat former lake bottom and sloping hillside composed of colluvium and loose, dry soils (lower hillslope). The survey was conducted using two 24-channel Geode exploration seismographs from Geometrics, Inc., with the accompanying SeisImager/2DTM software suite for in-field monitoring of data quality. To increase the signal-to-noise ratio, 8–10 shots were stacked (averaged) using a 6-kg sledgehammer striking a 2-cm thick, circular (30 cm diameter) stainless steel plate at 12 locations along each line.

Selected first arrival times (in ms) were generally limited to geophones overlying the lower hillslope, as the organic-rich, saturated sediments of the wet meadow resulted in lower signal-to-noise ratios by signal attenuation—Fig. S1 of the electronic supplemental material (ESM). Geophones overlying the saturated, peaty sediments exhibited low signal-to-noise ratios and therefore these regions of the velocity models contain less information; additionally, sustained winds likely contributed to noise in the data set. A combination of low pass and band pass filters were used to identify and manually pick the first arrivals for each channel. Using the principle of reciprocity, which states that p-wave travel times are equivalent upon the interchange of point source and receiver positions (Zelt and Smith 1992), the average reciprocal pick error was 1 ms for line SRT-south and 3 ms for line SRT-north.

For the final inversions, a two-layer gradational starting model was assigned for both SRT-south and SRT-north, transitioning from 400 m s^{-1} at the surface to 2,500 m s^{-1} at 10 m in depth, with a maximum depth assigned at 25 m for each model. The first arrival times were processed using Geogiga's DW Tomo software, which employs ray tracing, also known as the "shortest path" method (Moser 1991) in the forward modeling step. The forward model is a synthetic data set of p-wave arrival times generated from a predefined model of subsurface velocity. The calculated arrival times are compared with those observed in the field, and the subsurface velocity structure is updated using a regularized inversion with smoothing constraints. The model domain consists of gridded cells with dimensions of 0.625 m × 1.25 m (horizontal by vertical). The smoothing (regularization) constraints allow the user to define the degree of heterogeneity desired in the final model. Smoothing lengths in the x- and z-directions were set to minimize artifacts and overfitting, while maintaining enough structure to resolve changes in lithology and/or saturation with depth. Under the assumption that the subsurface consists of horizontal or near-horizontal lacustrine sedimentary deposits, 5.0-m-horizontal and 1.3-m-vertical smoothing constraints were selected for the final model runs. Iterations of forward and inverse modeling were carried out until the difference between observed and synthetic travel times were minimized.

It is possible that some portions of the inverted tomogram will be highly dependent on the starting model, rather than the actual arrival times. Interpretation should be limited to regions of the model that remain relatively unchanged when different starting models are used. To characterize these uncertainties, a sensitivity analysis was used to determine regions of the 2D tomogram that were dependent more on the data than the assigned starting model. To accomplish this, 22 separate inversions were carried out using distinct starting models that encompass reasonable assumptions about the subsurface p-wave velocity distribution and depth to bedrock (Table S1 of the ESM). The starting models consisted of a surface velocity of 500 or 1,500 m s^{-1}, gradationally increasing by 5-m increments downward toward a bedrock velocity of 5,000 m s^{-1} (Table S1 of the ESM). The depth to bedrock in the starting models was varied from 10 to 60 m in depth. If model cells exhibit little variability despite diverse starting model structures, they can be considered sensitive to the data and reliable for interpretation. For both seismic lines SRT-south and SRT-north, the 22 models converged in fewer than 10 iterations and resulted in root mean squared error between 2 and 10%. For each model cell, the coefficient of variation was calculated by dividing the standard deviation of the 22 resulting velocities in each cell by their mean.

Passive seismic

The horizontal to vertical spectral ratio (HVSR) technique is a passive seismic method (i.e. no active source such as a hammer is used) in which directional (north–south, east–west, up–down) components of ambient seismic noise are recorded in time series by a single station seismometer. The ratio of the horizontal to vertical frequency spectra are used to determine resonance frequencies of the underlying sediment, which varies with total sediment thickness under certain physical conditions (Nakamura 1989). HVSR methods are widely used in hydrogeology to characterize sediment thickness (e.g. Briggs et al. 2018; Sauret et al. 2015), given that the unconsolidated overburden and underlying bedrock interface contrast in acoustic velocity by a factor of 2 or more (Lermo and Chavez-Garcia 1994). Six HVSR surveys were conducted in the Quilcayhuanca Valley in August of 2016 using a Tromino multicomponent seismic recorder with acquisition lengths ranging from 15 to 45 min and sampling rate of 128 Hz. Irregularly spaced, the locations of the HVSR survey points were determined by the apparent quality of coupling to the ground surface using short metal spikes, and reasonable shielding from nearby livestock and high sustained winds.

The data were processed using the software capabilities of Grilla (Tromino) and Geopsy, which was developed as a part of the larger SESAME European Project (Site Effects Assessment Using Ambient Excitations, Bard 2004) After manually filtering out transient signals and applying 20-s windows to the time series, each windowed component was transformed to Fourier amplitudes, and the ratio of the horizontal to vertical amplitudes were calculated and averaged.

When the depth to bedrock is unknown, the estimated shear wave velocity of the unconsolidated sediment can be used to calculate overall sediment thickness (Johnson and Lane 2016). Resonance frequencies calculated for each point of measurement were converted to a range of likely bedrock depths (based on potential V_s), according to Eq. (1).

$$Z = \frac{V_s}{4\ F_0} \tag{1}$$

where Z is the depth (m) from the land surface to the bedrock or other competent surface, V_s is the average shear wave velocity structure (m s^{-1}) of the overlying sediment column, and F_0 is the H/V resonance frequency (s^{-1}, determined in HVSR data processing) where H and V are the vertical and horizontal components of ambient noise, respectively. As the average shear-wave-velocity structure of the unconsolidated sediment is unknown, first estimates were made to begin to constrain the overall sediment thickness. Typical lacustrine clays and gravels have exhibited V_s ranges of 200–500 m s^{-1} in published studies (L'Heureux and Long 2016; Jongmans et al. 2009). The presence of a clast supported talus body should increase these averages because rock material has a high stiffness and contributes to higher shear wave velocities of over 800 m s^{-1} (Brocher 2005).

Electrical resistivity tomography (ERT) and vertical electrical soundings

Seven ERT surveys were carried out in August of 2016 in the lower Quilcayhuanca meadow to complement information from the seismic surveys, targeting the upper 10 m of sediment (Fig. 2). Geoelectrical methods are among the most widely used geophysical methods for hydrogeological characterization because they can detect changes in subsurface saturation, porewater and groundwater conductivity, lithology, and clay content (e.g. Parsekian et al. 2015 and references therein). Because a combination of these factors contributes to bulk resistivity, interpretation can have a high degree of ambiguity. This ambiguity is reduced by combining the interpretation with other geophysical methods and borehole data. In general, higher degrees of saturation, along with clay content and smaller grain sizes contribute to a more electrically conductive subsurface, whereas larger fragments, crystalline rocks, and voids lead to higher resistivity. Electrical resistivity tomography surveys and vertical electrical soundings (VES) provide information about the subsurface electrical conductivity structure and are considered complementary to seismic methods, which provide information about elastic properties (Draebing 2016).

Using SuperSting R1/IP instrumentation (Advanced Geosciences, Inc.), ERT data were collected with 28 stainless steel electrodes placed at 6-m intervals for lines E1–E6 ("deep" surveys), as well as a single 3-m spacing roll-along survey (RA1, "shallow") that doubles over line E1, resulting in transect lengths of 162 and 144 m, respectively (Table 1). A roll-along survey is a way to overlap data from consecutive lines to increase survey length, but not depth of investigation, and was selected to cover the length of line E1. The roll-along survey data were merged with the deeper E1 survey to improve data density across the piezometer transect, and the merged data were inverted and are presented here as model E1*. To ensure low contact resistance between electrodes placed in the ground, electrode locations were watered with a saline solution until contact resistance test readings were well under 4,000 Ω, allowing the current to sufficiently flow into the subsurface. ERT surveys did not extend onto the lower hillslope due to very dry porous soil conditions, which resulted in high-contact resistance. Instead, all seven ERT surveys were conducted on the low-gradient valley floor. DC current was injected with 1.2-s signal pulse duration using a dipole-dipole electrode configuration, where the current source/receiver (A, B) and potential (M, N) electrode pairs are coupled adjacent to one another. The dipole-dipole array was chosen for this study to maximize the depth of investigation; it provided a maximum density of data points without compromising battery duration. The assignment and switching of dipole pair (source and receiver) combinations was specified and automated by using the SuperSting SwitchBox. Two measurements were stacked for each source-receiver combination and averaged in with a third measurement if the first two differed by more than 2%. The apparent resistivity values obtained in the field were inverted using the smooth model inversion from EarthImager 2D software (Advanced Geosciences, Inc.). A smoothing multiplier of 10 was used as a constraint on the ERT inversions. This is a Lagrange multiplier in the objective function that determines the degree of roughness in the model, a value of 10 being the recommended setting for surface data (Advanced Geosciences, Inc. 2009). Model convergence criteria were set such that differences between measured and calculated resistivity values exhibit root mean square errors less than 10%.

Using a starting model of the average apparent resistivity in each line, all six electrical resistivity tomography models converged within 1–5 iterations with a root mean squared (RMS) error between predicted and measured data less than 5%, and normalized L2-norm values below 0.3 (Table 1). The normalized L2-norm is a measure of data misfit, as the squared difference of weighted errors between the synthetic and modeled data, normalized by the total number of data points. Horizontal resolution was set to half the electrode spacing, 3 m for the deep survey and 1.5 m for the shallow roll-along. Vertically, the model cell size increased from 2 m at the surface to 4 m at depth. Because the deeper E1 survey and the shallower roll-along were performed on two different days that had distinct soil moisture conditions and varying contact resistance, 91 shallow data points out of a total of 1,013 were removed that coincided with more than 3% difference in resistance between lines RA1 and E1. Repeated measurements show little to no noisy data points on surveys E2–E6 and no data points were removed for these lines.

The depth of investigation (DOI) indexing method (Oldenburg and Li 1999) was used to determine the depth below which the 2D resistivity model is no longer reliable. This was achieved by performing each inversion with two divergent, homogeneous half-space starting models and computing the normalized difference between the two resistivity values for each model cell. Model cells resulting in a DOI index greater than 0.1 were not plotted for interpretation and were considered more reliant on the starting model than on the data.

Vertical electrical soundings

One-dimensional (1D) VES methods are among the simplest near-surface geoelectrical methods, and can be advantageous for use in remote alpine environments where deep probing of the subsurface structure is desired (Bechtel and Goldscheider 2017). Although VES only provides models of resistivity in the vertical direction without consideration of two-dimensional (2D) or three-dimensional (3D) influences and anomalies, the method was chosen for this study because the maximum separation allowable by the VES cables increases the depth of investigation from the shorter 2D ERT surveys. Because VES requires the assumption that the subsurface consists of horizontal homogeneous layers, resulting models reveal the simplest resistivity structure possible and can be presented as resistivity and depth ranges, as opposed to detailed models of subsurface electrical structure that vary laterally (Kneisel 2004).

For this study, six VES soundings were performed on the center of each ERT line using a Schlumberger array, where the current injection and receiver electrodes (electrodes A, B)

Table 1 Survey and model conversion details for 2D resistivity and seismic lines

2D line	Survey length (m)	Receiver spacing (m)	No. of data points used	Data misfit	
				RMS (%)	L2 norm
E1*	162	NA	1,013	3.87	0.29
RA1	144	3	NA	NA	NA
E1	162	6	NA	NA	NA
E2	162	6	346	3.86	0.15
E3	162	6	346	3.41	0.12
E4	162	6	346	3.39	0.12
E5	162	6	346	4.4	0.19
E6	162	6	346	5.02	0.25
SRT-south	117.5	2.5	354	3.58	NA
SRT-north	117.5	2.5	335	5.33	NA

Data misfit represented as both the root mean square error (RMS) and L2 norm, as the weighted sum of squared differences between observed and predicted values. Conversion information listed as NA (not applicable) is noted for merged values RA1 and E1, whose combined data sets became E1*. Seismic refraction model conversion error is represented as RMS only

were placed on either side of the voltage (potential) electrodes M and N. The maximum AB electrode separation varied from 150 to 300 m, depending on the length of accessible terrain in the study area (Table 2). Theoretically, the depth of investigation for each sounding depends on the maximum electrode separation and the conductivity of the subsurface. In this case, the maximum DOI for an AB separation of 300 m is between 30 and 90 m, although these depths can be reduced with lower ground resistivity and decreased signal strength (Edwards 1977).

Each sounding was conducted by manually relocating the source and receiver electrodes after each measurement to a spacing that varied logarithmically from 2 m to the maximum available separation distance, consisting of up to 18 manual data collection points. When the inner potential electrodes (M and N) were repositioned to wider spacing, repeat measurements were taken at the previous and new MN locations to account for data offset. The VES apparent resistivity data were inverted using EarthImager 1D software (Advanced Geosciences, Inc.), which employs a damped least squares method to construct a layered resistivity model, where the number of layers were minimized according to data fit. All

Table 2 Maximum current source and receiver electrode spacing (AB), and model convergence for 1D vertical electrical soundings (VES)

1D sounding	Maximum AB separation (m)	Data misfit (RMS %)
V1	144.8	4.93
V2	300	0.91
V3	144.8	9.73
V4	261	2.89
V5	300	3.13
V6	144.8	2.01

1D resistivity profiles converged with less than 5% RMS data misfit between observed and modeled values, with the exception of V3, which converged with nearly 10% misfit (Table 2).

Results and interpretation

The geophysical data, sections, and soundings revealed a heterogeneous near-surface distribution of material and/or saturation at depths coinciding with lithological interfaces shown in borehole logs. Results from each geophysical method are presented separately, and interpreted jointly along with borehole data to conceptualize changes in lithology and saturation with depth.

Seismic refraction tomography

Results from the starting model sensitivity analysis show large variations in the portions of the model that are deeper and closer to the valley center, where signals were attenuated in the peaty organic soil (Fig. S2 of the ESM). In both lines SRT-south and SRT-north, the upper 10 m varied by 10% or less, and can be considered sensitive to the data. Deeper regions of the models and those toward the center of the valley were more sensitive to the starting model scenarios, and varied by 15–35% between model sensitivity runs below depths of ~10 m. These lower regions of the model are considered unreliable and are excluded from analysis in this study.

The final SRT-south model converged after 10 iterations with a fitting error of 1.97 ms, and SRT-north model converged after 10 iterations with a fitting error of 3.15 ms. Two dominant seismic velocity ranges were observed under lines SRT-south (Fig. 4a) and SRT-north (Fig. 4b), with shallow areas being relatively slow (500–700 m s^{-1}) and faster velocities at depths >5 m (2,000–3,000 m s^{-1}). The reliability of the velocity models was considered using reconstructed seismic raypaths that are based on the shortest travel time connecting each source to each receiver along the line (Fig. 4a,b). Regions where many raypaths intersect are considered to be well constrained by the data (arrival times), whereas regions that lack raypaths are interpolations and were not considered for interpretation. In models SRT-south and SRT-north, dense intersections of modeled raypaths in the top 10–15 m overlap with the clay-boulder interface at depth, although piezometer GW1 extends into regions of moderate variation (5–10%, Fig. 4).

The slower velocities (500–700 m s^{-1}) that were closest to the surface toward the valley side (Fig. 4a) were consistent with other studies of talus slopes in North America (e.g. Brody et al. 2015), and can be associated with porous, unsaturated coarse sediments (Powers and Burton 2012). The lower hillslope produced strong audible reverberations after striking the sledge hammer. Because the hillslope comprised large boulder-sized clasts (0.5–2 m in diameter) that were partially exposed above dry soil, the slow velocities in zone 1a are interpreted as an unsaturated, highly porous colluvial deposit. At the base of the slope, similar velocities were observed in the partially saturated, organic and clay-rich sediments that exhibited low resistivity (Figs. 4a and 6b; zone 1), which were devoid of any fragments or clasts represented in the borehole logs (Chavez 2013). Slow velocities in zone 1 appear to correspond to both the lower hillslope and to the fine-grained, variably saturated lacustrine sediments immediately underlying the valley floor.

At depths of 5–10 m, the 1,300 m s^{-1} iso-velocity contour (Fig. 4c,d) corresponds to depths where boulders were encountered in the boreholes (Chavez 2013). Below this line, the faster seismic velocities (2,000–3,000 m s^{-1}) are consistent with more compact, dense, and/or saturated media, likely reflecting the top of a buried, clast-supported body of talus with a higher overall seismic velocity. The composition of the sediment infilling the talus boulders could not be determined by seismic methods, and was explored using electrical methods (see section 'Electrical resistivity tomography'). The vertical change in seismic velocity was plotted for each column of model cells, showing a step-increase in p-wave velocity with depth, rather than a gradational increase (Fig. 4c,d). The transition to faster seismic velocities occurs 5–10 m beneath the surface, and borehole observations above this transition at GW 7 are absent of any clasts or fragments. These lines of evidence indicate that zone 1 is a laterally continuous unit of fine-grained lacustrine sediments lying beneath the colluvial slope (zone 1a), and that the refracting interface that corresponds to 1,300 m s^{-1} does not appear to be a subsurface extension of the lower hillslope (Fig. 4c; zone 1).

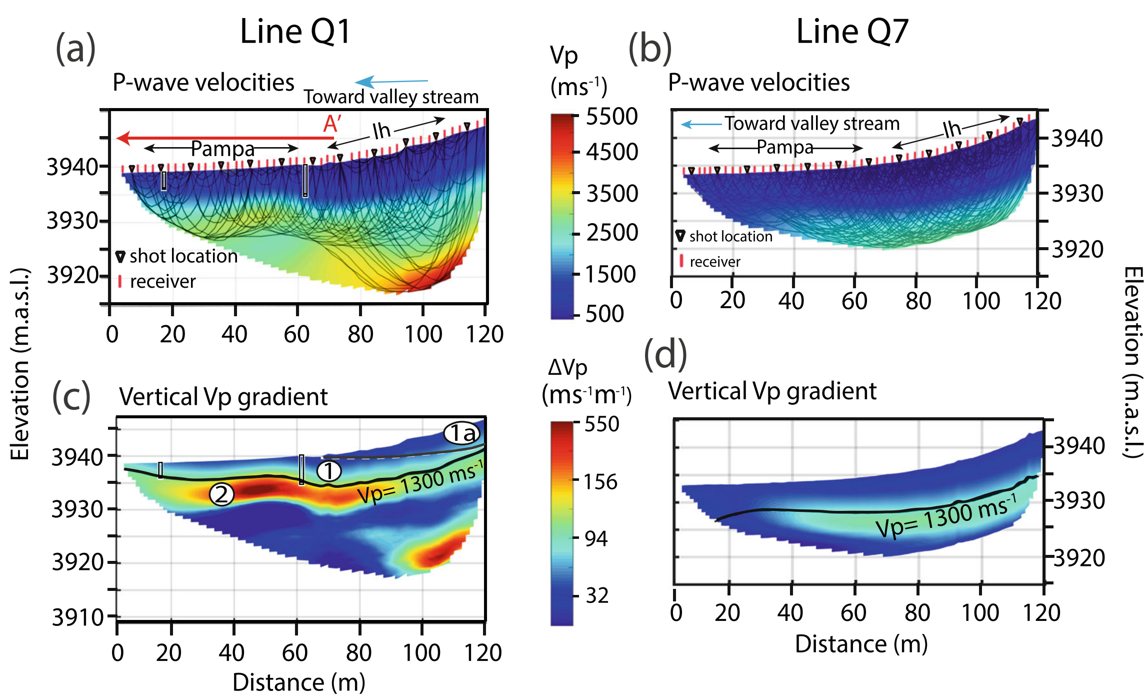

Fig. 4 **a** P-wave velocity model, showing modeled raypaths as small black lines. Piezometer depths for GW7 and GW1 included for reference. **b** P-wave velocity model and raypaths for line SRT-north. **c** –**d** Change in velocity with every vertical meter for lines SRT-south and SRT-north. **c** Shows hydrogeologic zones 1a, 1, and 2. The thick black line represents the 1,300-m s^{-1} contour, which coincides with the depth of drilling refusal. Topography labeled as lower hillslope (lh) and relatively flat pampa (wet meadow)

Electrical resistivity tomography

The depth of investigation of the 2D resistivity surveys limits interpretation to the top ~20 m of sediment. Models of subsurface resistivity across the wet meadow indicate a region of varying resistivity (100–300 Ωm) in the shallow subsurface (Fig. 5a; zone 1), where lacustrine clays and silts were encountered during drilling and p-wave velocities are relatively slow. The upper, more electrically conductive (Fig. 5a, zones 1 and 2, 50–300 Ωm) portion of the subsurface transitions to a higher resistivity zone (Fig. 5a, zone 3, 300–650 Ωm) at 10–15 m depth. Zones 1, 2 and 3 are present in all six ERT lines and show spatial continuity (Fig. 5b), suggesting variable layer thicknesses and moisture content.

Low to moderate values (10–300 Ωm) in the uppermost 5 m of sediment, which are dominated by lacustrine clays, are likely attributed to variable saturation and/or composition. The surveys were conducted during the dry season, and evaporative moisture deficits in the near surface could explain these variations. Further, this variability can be influenced by unsaturated pore spaces and the presence of sand particles, which would contribute to elevated resistivity readings from the background conductive clays (Samouëlian et al. 2005).

Vertical electrical soundings

The top 7 m of valley fill for each VES point measurement varied from 150 to 3,000 Ωm, and deviated from 2D values at similar depths (Fig. 6). Because the survey was conducted toward the peak of the dry season (late July/early August), spatially variable soil moisture conditions along with composition may contribute to higher variability in the shallow layers (Michot et al. 2003). The VES profiles are generally consistent with the ERT sections, showing: (1) high and variable resistivity (up to 1,000 Ωm) at the shallowest depths of less than 5 m (zone 1); (2) lower resistivity (50–200 Ωm) at depths of 5–10 m (zone 2); and (3) higher resistivity (300–600 Ωm) in regions at depths greater than 10 m (zone 3). All VES profiles show that the resistivity subsequently decreases at depths of 18–35 m below land surface (Fig. 6; zone 4). This deeper, less resistive layer could be composed of subglacial till deposits. Low-resistivity till layers are common in alpine glacial valleys, particularly when fully saturated and with a high clay content (e.g. Andersen et al. 2016; Brand et al. 1987; Kneisel 2004).

Further constraints from the VES data also suggest that zone 3 is not indicative of bedrock. These lower resistivity values (50–200 Ωm) in zone 4 (Fig. 6) can be explained by the presence of a deeper unit composed of older lacustrine deposits or clay-rich glacial till, rather than bedrock. Thick glacial deposits above bedrock are prevalent throughout the proglacial valleys of the Cordillera Blanca upon glacial retreat (Chavez 2013; Klimeš 2012; López-Moreno et al. 2016) and are consistent with the decrease in resistivity at depth in the vertical electrical soundings, provided the glacial deposits contain electrically conductive material. The lower extent of the Quilcayhuanca talus aquifer therefore lies at the top of zone 4, leading to an overall aquifer thickness ranging from 10 to 25 m. Further investigation into deeper sediments is needed to corroborate the lower portions of the VES models because geophysical methods used in isolation could produce artifacts and uncertainties, as well as multiple solutions for the same data set, especially with increasing depth where signal strength decreases (Barker 1989).

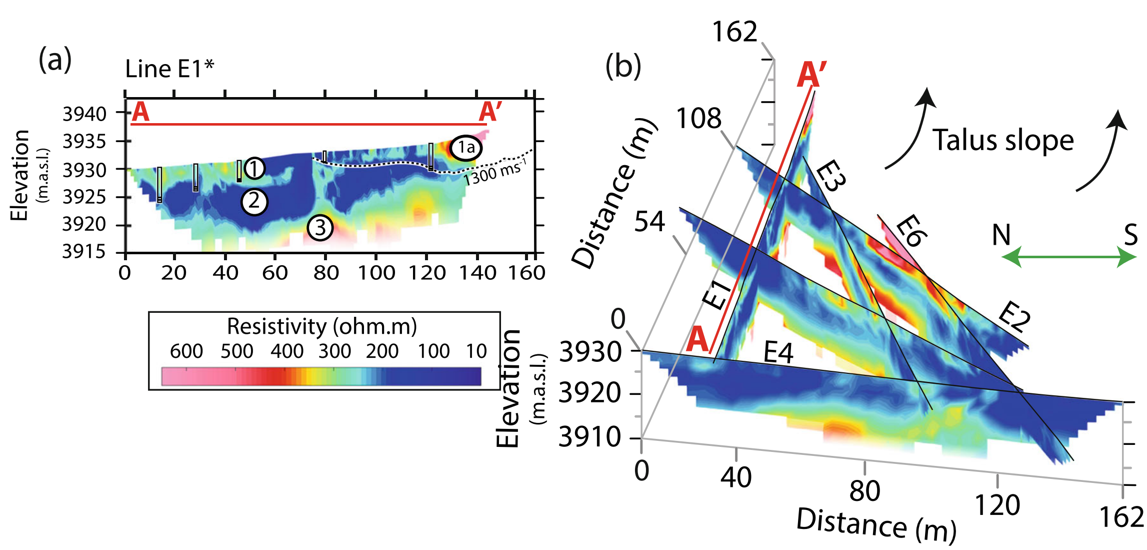

Fig. 5 **a** 2D resistivity section for line E1*, which consists of merged data from E1 (6-m spacing) and RA1 (3-m spacing roll-along survey). Four hydrogeologic zones (1a, 1, 2, and 3) are marked, along with the 1,300 m s^{-1} p-wave velocity contour (dotted line). **b** All six intersecting resistivity models plotted in 3D

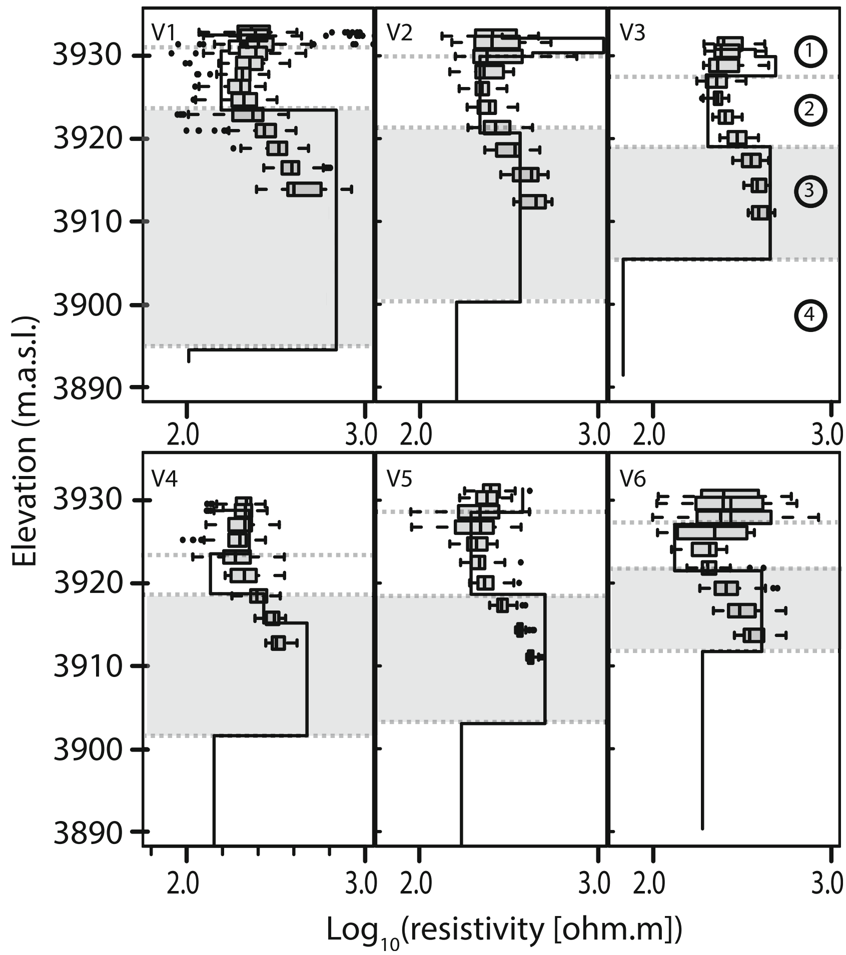

Fig. 6 1D resistivity plotted with depth (solid line), indicating zones of substantial aquifer storage (shaded area). 2D ERT resistivity represented as box plots for each model row, plotted at the mean row depth. Hydrogeologic zones 1, 2, 3, and 4 are marked on the upper right

Passive seismic

Clear resonance frequency peaks were found for all six HVSR survey points, ranging from 1.82 to 3.73 Hz (Fig. 7b). The peak and trough shape of the resonance frequency curves indicate a high acoustic impedance contrast of the underlying material, likely due to a competent bedrock-sediment interface (Seht and Wohlenberg 1999). Given that the measured *H*/*V* resonance frequencies ranged from 2 to 4 Hz (Fig. 7b), and assuming a V_s structure that ranges from 300 to 600 m s^{-1} for clays intermixed with gravel or boulder-sized fragments and glacial deposits, one can estimate a range of bedrock depths (Fig. 7a). Estimated average shear wave velocities in the range of 300–400 m s^{-1} correspond to bedrock depths ranging from 20 to 50 m, while a V_s range of 500–600 m s^{-1} indicates that bedrock is between 30 and 85 m, depending upon the location in the valley.

Discussion

Results integrated from four geophysical methods along with borehole data present a refinement of the conceptualized hydrogeologic structure and function of the Quilcayhuanca lower hillslope and wetland zones (Fig. 8). The conceptual model supports that recharge that is sourced primarily from precipitation occurs at the lateral valley edge where talus boulders are exposed, although portions of this recharge could be sourced from a small ice patch that lies directly upslope. Laterally recharged water becomes confined as it flows toward the valley center, and emerges in valley springs via preferential flow pathways. Proglacial depositional environments generally exhibit a high degree of spatial complexity (Carrivick et al. 2013); however, the Quilcayhuanca and other valleys of the range contain organized structure that originates in lacustrine deposition (Glas et al. 2018). The conceptual model posits that these low-permeability lacustrine sediments contain and slow groundwater discharge to perennial springs throughout the dry season.

Prior work indicates the springs that emerge at the interface of the talus slope and the valley floor are chemically distinct from glacial meltwater, sharing more hydrochemical properties with springs toward the center of the valley (Baraer et al. 2015). These springs are likely connected to the talus aquifer via macropores in the clay structure of the aquitard, which can

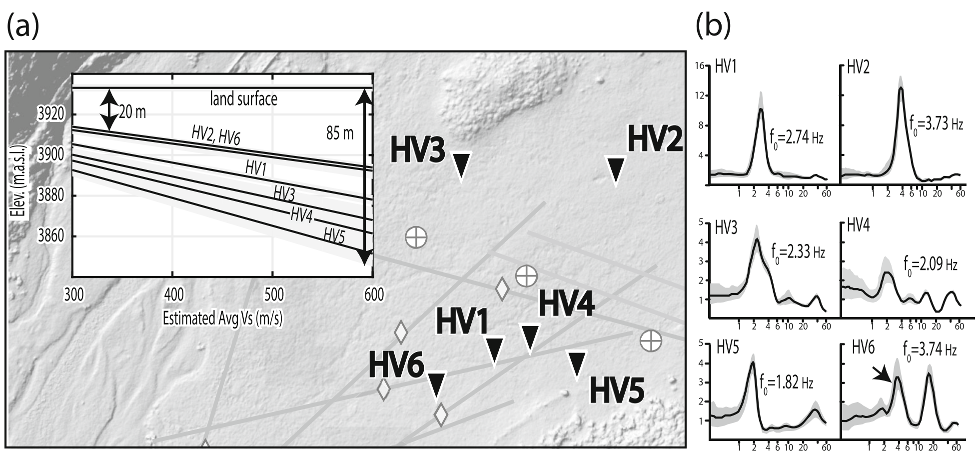

Fig. 7 **a** Spatial locations of HVSR points in relation to other geophysical lines (background). Plot inset: Possible sediment thicknesses for each HVSR point based on estimated shear-wave-velocity ranges. **b** HVSR plots for all six locations. Standard deviation of *H*/*V* ratios in shaded grey region. Resonance frequency for each point is marked as f_0. (Aerial imagery from Wigmore and Mark (2017) Department of Geography/Byrd Polar and Climate Research Center, The Ohio State University, Columbus, OH, USA)

transmit artesian groundwater to the land surface (Dekker and Ritsema 1996; Kurtzman et al. 2016). Because these pathways hypothetically have lower levels of clay than their surroundings, they may contribute to bulk resistivity values that are slightly higher (200–300 Ωm) than the surrounding lacustrine clays (50–200 Ωm in zone 2). The locations of springs and the tributaries they feed remained largely unchanged interannually, suggesting that the preferential flow pathways that lead to those tributary positions are also perennial.

Borehole observations indicate the presence of crystalline boulders at depths corresponding to areas with low bulk resistivity (50–200 Ωm). The presence of large crystalline rock fragments, however, are more likely associated with higher resistivity values, depending on the extent of saturated

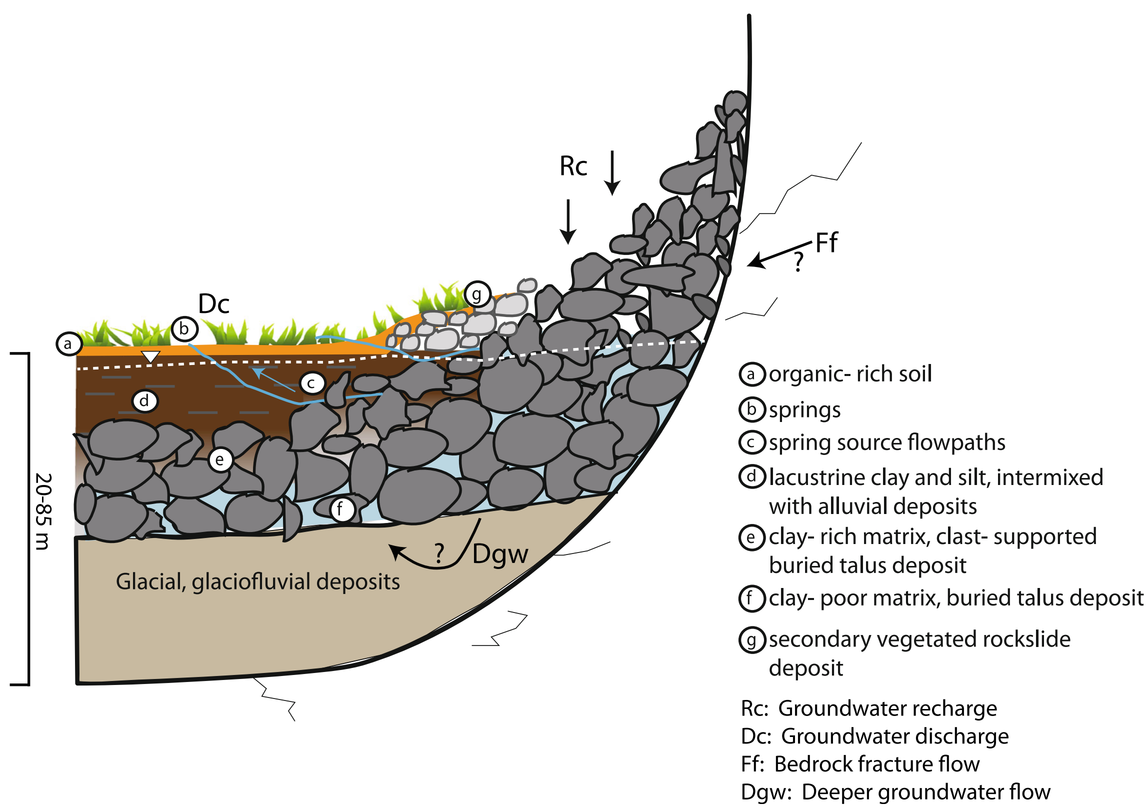

Fig. 8 Conceptual model of Quilcayhuanca talus aquifer, including recharge zones at valley edge and zones of maximum storage

fractures and weathering within the clasts (Loke 2000; Samouëlian et al. 2005). The low resistivity in the presence of boulders in zone 2 suggests that the sediments infilling the talus are saturated and clay-rich, contributing to a lower bulk permeability of the unit. The small grain size and conductive electrical properties of clay along with saturated pore spaces can mask a more resistive signal from large igneous rock fragments (Abu-Hassanein et al. 1996). This agrees with evidence from piezometers that, in the dry season, moisture content and saturation are variable near the surface, but full saturation occurs at depths corresponding to the buried talus.

Quilcayhuanca, which is geomorphologically similar to many northern and central valleys of the Cordillera (Glas et al. 2018), contains talus slopes that are incident on the pampa floor at an angle of 20–35°, becoming buried beneath the less permeable lacustrine sediments. The top of the buried talus unit coincides with the 1,300 m s^{-1} p-wave velocity contour, and this interface extends continuously eastward and upward toward the valley edge. The buried unit, therefore, is likely connected to an exposed portion of talus near the valley wall, recharging groundwater to deeper confined sediments during times of precipitation.

The uppermost portions of the buried talus at depths of 2–10 m are infilled with saturated clay, contributing to a low (10–100 Ωm) bulk resistivity (zone 2). The region of higher resistivity (zone 3) is interpreted to be a continuation of the buried talus deposit at depth, but infilled with a clay-poor matrix due to limited infiltration of lake bottom sediments into the talus material at the time of deposition. The lack of clay in deeper portions of the talus deposit suggests that the sediments in Quilcayhuanca's lower meadow are more permeable between depths of 10–25 m, contribute to a higher hydraulic conductivity, and form the productive aquifer storage volume. An alternative hypothesis for the increase in resistivity at depths of 10–15 m is that this boundary is the top of intact or weathered bedrock, rather than unconsolidated material. Bedrock depth ranges of 20–85 m, which were estimated from the HVSR results, do not support this alternative hypothesis. In order for bedrock depths to be this shallow, overlying shear wave velocities would range from 200 to 300 m s^{-1}, which is more consistent with soft soils and stiff clays with less than 20% gravel or rock fragments (Borcherdt and Glassmoyer 1994).

Geomorphological evolution

Results from the geophysical surveys indicate that Quilcayhuanca and other pampas of the Cordillera Blanca underwent lacustrine phases in which high amounts of colluvium (talus and debris fans) were deposited on lake floors from steeply incised proglacial valley walls. This process is currently taking place elsewhere in the range, where fine-grained lake sediments are deposited with talus boulders such as in the Llanganuco pampa (Glas et al. 2018). Over time, glacial lake infilling and deposition of fine-grained lake sediments occurred over the subaqueous talus, with the lake draining slowly enough to allow for thick lacustrine clay deposition that infiltrated the upper 5–10 m of the talus deposit. The fine-grained and relatively impermeable sediment matrix in the upper talus then continued to infill, resulting in 2–8 m of clay that is devoid of clasts or fragments in the shallowest portions.

Deeper parts of the talus deposit that were not directly exposed to the water column became a lower layer of the talus structure that has a clay-poor matrix and is more hydraulically conductive (Fig. 8). After the terrestrialization of the Quilcayhuanca Valley lake since the last glacial retreat ~12 ka (Rodbell et al. 2008), the accumulation of peat-rich organic soils accumulated by the process of paludification, which generally occurs over moist mineral soils and leads to conditions of poor drainage (Lavoie et al. 2005). Both peaty and peat-poor organic soils are commonly found in the valley pampas of the Cordillera Blanca (Polk 2016), as are terrestrial and subaqueous talus deposits in the many lakes of the range (Emmer et al. 2016; Vilímek et al. 2015). Cordillera Blanca slope deposits submerged in alpine lake environments are therefore the primary stage for the formation of confined aquifers upon the lakes' paludification or terrestrialization, and are likely found in other valleys of the range. Furthermore, because alpine proglacial wetlands occur globally (Jacobsen et al. 2012), talus aquifers likely influence the global hydrologic cycle by buffering interannual streamflow fluctuations caused by seasonal precipitation regimes.

Seismic velocities directly beneath the lower hillslope were similar to those found in zone 1 (500–700 m s^{-1}), and the sediment column directly at the toe of the lower hillslope was completely devoid of clasts. It does not appear that the lower hillslope connects with the buried talus aquifer, as these two units are separated by ~5 m of clay sediments. This indicates that the exposed colluvial slope at the valley edge was not deposited at the time of the buried talus layer, but rather after deposition of the organic and clay-rich lake sediments.

Groundwater storage potential

Although this study has examined only a single talus aquifer, a first-order, rough approximation of the drainable groundwater storage potential of the Quilcayhuanca Valley can be made under assumptions of similar depth and porosity throughout both of its wet alpine meadows, which cover approximately 3% of total catchment area above 3,800 masl (Gordon et al. 2015). The geophysical interpretations support that a confined talus aquifer underlying the lower Quilcayhuanca meadow is 10–25 m thick. If confined talus aquifers of comparable thickness underlie the entire 1.86 km^2 of the wet meadow area in the Quilcayhuanca Valley above 3,800 masl, the total aquifer volume would be approximately 0.02–0.05 km^3. This is an overestimation of pampa area coverage because varied proportions of the wet meadow do not contain talus, nor are they covered by cross-valley moraines that have been found to transport and exchange groundwater with the surface, rather than store it (Gordon et al. 2015). Using a typical porosity of coarse-grained talus deposits (30–40%), one could estimate that talus aquifers in the Quilcayhuanca Valley can store from 0.006 to 0.02 km^3 of groundwater. This calculation varies greatly with porosity estimates, and further work is needed to constrain this value as well as the spatial distribution of these aquifers.

To put this storage capacity into context, consider the basin-wide precipitation and discharge for comparison. The outflow of the Santa River at the La Balsa gage, which drains the Callejon de Huaylas basin, discharges 2.8 km^3 annually (1954–1997, Mark and Seltzer 2003). Hence, the Quilcayhuanca meadows have the capacity to store between 0.2 and 0.7% of the upper Santa's annual basin discharge, under the assumption of a 30–40% aquifer porosity. Assuming an annual precipitation rate of 650 mm/year for the Callejon de Huaylas (Huaraz station, 3,052 masl, Mark and Seltzer 2003), the Quilcayhuanca talus aquifers have the capacity to store 0.2–0.6% of annual precipitation for the basin, although it is likely that only a portion of this groundwater turns over on decadal timescales.

This study estimates that the clay-rich aquitard in Quilcayhuanca's talus aquifer is approximately 10 m thick, with a depth to crystalline bedrock between 20 and 85 m. These estimates can be used to constrain boundary conditions for groundwater flow models in order to calculate groundwater residence times using particle tracking techniques (Pollock 1989). More work is needed to characterize the nature of deeper sediments in talus aquifers, which will improve estimates of porosity at depth. Because this region is remote and deeper drilling operations are not feasible, combined remote sensing and geophysical methods provide a means to understand the composition and structure of these deeper sediments. Additionally, these talus aquifers are likely intermittent in some valley pampas, and surveys are needed to map the occurrence of sloping talus and springs to better refine their spatial extent. In addition to a spatial characterization, further investigation is needed to quantify any glacial melt contributions to aquifer recharge in these alpine groundwater systems. These glacial contributions to stored groundwater will likely diminish over the next few decades, particularly if the source glacier is low-lying and small.

Conclusion

Four near-surface geophysical methods were employed and interpreted with existing borehole records to estimate aquifer thickness and composition in the Quilcayhuanca Valley. Results suggest that the top of a buried talus unit lies 2–8 m below the surface, and the shallower portion of the talus is infilled with lacustrine clay. Groundwater is likely stored beneath this low permeability layer in clay-poor talus at depth, as the bulk resistivity of the subsurface increases in these deeper portions. Groundwater likely discharges to the surface through preferential flow paths that penetrate the surficial material, forming springs that flow to the valley stream throughout the region's wet and dry seasons. The talus aquifers of the Cordillera Blanca formed from the interaction of lake sediment deposition with gravitational slope deposits. Glacial retreat and prevalent landslides have led to the formation and damming of many alpine lakes throughout the range, many of which have filled with fine sediments over time. These lake deposits act as a confining layer over saturated buried talus, which existed in a subaqueous environment. The lack of frozen material at depth allows for greater groundwater storage volumes and exchange with surface waters than alpine groundwater flow that is controlled by permafrost or seasonal freeze–thaw patterns.

Based on this study and assumptions of aquifer porosity, it is estimated that the maximum pampa storage capacity of the Quilcayhuanca Valley above 3,800 masl is between 0.006–0.02 km^3. Refinement of this estimate will allow for basin-wide calculations of hydrologic processes in a region that is becoming increasingly water-stressed, including groundwater residence times in these valleys. Future work should be aimed at refining the storage capacity and permeability of deeper sediments and evaluating the spatial extent of buried talus aquifers that likely occur where large talus deposits intersect proglacial wetlands and grasslands, as evidenced by the presence of spring-sourced tributaries. The talus aquifers of the Cordillera Blanca represent a hydrogeologic system that relies on interactions between glacial erosion, gravitational slope deposits, and the formation and sedimentation of proglacial lakes in a tropical climate. The water from these aquifers will become an increasingly important source of dry season discharge for the Callejon de Huaylas basin over the next few decades, when many of the glaciers of the range are predicted to disappear.

Acknowledgements The authors would like to thank Martin Briggs, Adam Emmer, William Kochtitzky, and an anonymous reviewer for improving the quality of this paper. Additionally we would like to acknowledge W. Steven Holbrook for instructional and technical support throughout the process of data collection and analysis.

Any use of trade, firm, or product names is for descriptive purposes only and does not imply endorsement by the US Government.

Funding information This material is based upon work supported by the National Science Foundation [Grant No. DGE-1449617 and EAR-

1316429]. Research for this project was also supported by a student research grant from the Geological Society of America and by the Syracuse University EMPOWER program.

References

Abu-Hassanein ZS, Benson CH, Blotz LR (1996) Electrical resistivity of compacted clays. J Geotech Eng 122(5):397–406. https://doi.org/10.1061/(ASCE)0733-9410(1996)122:5(397)

AGI (2009) Instruction Manual for EarthImager 2D version 2.4.0. Advanced Geosciences, Inc, Austin, Texas, p 139

Ames A (1998) A documentation of glacier tongue variations and lake development in the cordillera Blanca, Peru. Z Gletscherkd Glazialgeol 34(1):1–36

Andersen TR, Westergaard JH, Pytlich A (2016) Delineation of fault systems on Langeland, Denmark based on AEM data and boreholes. ASEG Extended Abs 2016(1):1-6

Baraer M, McKenzie JM, Mark BG, Bury J, Knox S (2009) Characterizing contributions of glacier melt and groundwater during the dry season in a poorly gauged catchment of the cordillera blanca (peru). Adv Geosci 22(22):41-49. https://doi.org/10.5194/adgeo-22-41-2009

Baraer M, Mark BG, McKenzie JM, Condom T, Bury J, Huh K-I, Portocarrero C, Gomez J, Rathay S (2012) Glacier recession and water resources in Peru's Cordillera Blanca. J Glaciol 58(207): 134–150. https://doi.org/10.3189/2012JoG11J186

Baraer M, McKenzie J, Mark BG, Gordon R, Bury J, Condom T, Gomez J, Knox S, Fortner SK (2015) Contribution of groundwater to the outflow from ungauged glacierized catchments: a multi-site study in the tropical Cordillera Blanca, Peru. Hydrol Process 29(11):2561–2581. https://doi.org/10.1002/hyp.10386

Bard PY (2004) The SESAME project: an overview and main results. In: Proc. of 13th World Conf. on Earthquake Engineering, Vancouver, BC, August, 2004, pp 1–6

Barker RD (1989) Depth of investigation of collinear symmetrical four-electrode arrays. Geophysics 54(8):1031–1037. https://doi.org/10.1190/1.1442728

Bechtel TD, Goldscheider N (2017) Geoelectrical fingerprinting of two contrasting ecohydrological peatland types in the Alps. Wetlands. https://doi.org/10.1007/s13157-017-0921-5

Borcherdt RD, Glassmoyer G (1994) Influences of local geology on strong and weak ground motions recorded in the San Francisco Bay region. US Geol Surv Prof Pap 77

Bradley RS, Vuille M, Diaz HF, Vergara W (2006) Threats to water supplies in the tropical Andes. Science 312(5781):1755–1756

Brand G, Pohjola V, Hooke RL (1987) Evidence for a till layer beneath Storglaciären, Sweden, based on electrical resistivity measurements. J Glaciol 33(115):311–314

Briggs MA, Lane JW, Snyder CD, White E, Johnson ZC, Nelms DL, Hitt NP (2018) Shallow mountain bedrock limits seepage-based headwater climate refugia. Limnologica. https://doi.org/10.1016/j.limno.2017.02.005

Brocher TM (2005) Compressional and shear wave velocity versus depth in the San Francisco Bay Area, California: rules for USGS Bay Area Velocity Model 05.0. 0. US Geol Surv Open File Rep 2005-1317

Brody AG, Pluhar CJ, Stock GM, Greenwood WJ (2015) Near-surface geophysical imaging of a talus deposit in Yosemite Valley, California. Environ Eng Geosci 21(2):111–127

Burns P, Nolin A (2014) Using atmospherically-corrected Landsat imagery to measure glacier area change in the Cordillera Blanca, Peru from 1987 to 2010. Remote Sens Environ 140:165–178. https://doi.org/10.1016/j.rse.2013.08.026

Bury J, Mark BG, Carey M, Young KR, Mckenzie JM, Baraer M, French A, Polk MH (2013) New geographies of water and climate change in Peru: coupled natural and social transformations in the Santa River watershed. Ann Assoc Am Geogr 103(October 2012):363–374. https://doi.org/10.1080/00045608.2013.754665

Caballero Y, Jomelli V, Chevallier P, Ribstein P (2002) Hydrological characteristics of slope deposits in high tropical mountains (Cordillera Real, Bolivia). Catena 47(2):101–116. https://doi.org/10.1016/S0341-8162(01)00179-5

Cardarelli E, Cercato M, Cerreto A, Di Filippo G (2010) Electrical resistivity and seismic refraction tomography to detect buried cavities. Geophys Prospect 58(4):685–695

Carrivick JL, Geilhausen M, Warburton J, Dickson NE, Carver SJ, Evans AJ, Brown LE (2013) Contemporary geomorphological activity throughout the proglacial area of an alpine catchment. Geomorphology 188:83–95

Chavez D (2013) Groundwater potential of pampa aquifers in two glacial watersheds, Cordillera Blanca, Peru. MSc Thesis, McGill University, Montreal

Chevallier P, Pouyaud B, Suarez W, Condom T (2011) Climate change threats to environment in the tropical Andes: glaciers and water resources. Reg Environ Chang 11(1):179–187

Clow DW, Schrott L, Webb R, Campbell DH, Torizzo A, Dornblaser M (2003) Ground water occurrence and contributions to stream flow in an alpine catchment, Colorado Front Range. Groundwater 41937e950(7):937–950. https://doi.org/10.1111/j.1745-6584.2003.tb02436.x

Dekker LW, Ritsema CJ (1996) Preferential flow paths in a water repellent clay soil with grass cover taken in close order over a distance of 195 cm at depths. Water Resour Res 32(5):1239–1249

Draebing D (2016) Application of refraction seismics in alpine permafrost studies: a review. Earth Sci Rev 155:136–152. https://doi.org/10.1016/j.earscirev.2016.02.006

Edwards LS (1977) A modified pseudosection for resistivity and IP. Geophysics 42(5):1020–1036

Emmer A, Klimeš J, Mergili M, Vilímek V, Cochachin A (2016) 882 lakes of the Cordillera Blanca: an inventory, classification, evolution and assessment of susceptibility to outburst floods. Catena 147:269–279. https://doi.org/10.1016/j.catena.2016.07.032

Farber DL, Hancock GS, Finkel RC, Rodbell DT (2005) The age and extent of tropical alpine glaciation in the Cordillera Blanca, Peru. J Quat Sci 20(7–8):759–776. https://doi.org/10.1002/jqs.994

Georges C (2004) 20th-century glacier fluctuations in the tropical Cordillera Blanca, Peru. Arct Antarct Alp Res 36(1):100–107

Giovanni MK, Horton BK, Garzione CN, McNulty B, Grove M (2010) Extensional basin evolution in the Cordillera Blanca, Peru: stratigraphic and isotopic records of detachment faulting and orogenic collapse in the Andean hinterland. Tectonics 29(6):1–21. https://doi.org/10.1029/2010TC002666

Glas R, Lautz L, McKenzie J, Mark B, Baraer M, Chavez D, Maharaj L (2018) A review of the current state of knowledge of proglacial hydrogeology in the Cordillera Blanca, Peru. Wiley Interdiscip Rev Water 5(5):e1299

Glasser NF, Clemmens S, Schnabel C, Fenton CR, McHargue L (2009) Tropical glacier fluctuations in the Cordillera Blanca, Peru between 12.5 and 7.6 ka from cosmogenic 10-Be dating. Quatern Sci Rev 28(27–28):3448–3458. https://doi.org/10.1016/j.quascirev.2009.10.006

Gordon RP, Lautz LK, McKenzie JM, Mark BG, Chavez D, Baraer M (2015) Sources and pathways of stream generation in tropical proglacial valleys of the Cordillera Blanca, Peru. J Hydrol 522: 628–644. https://doi.org/10.1016/j.jhydrol.2015.01.013

Haeberli W, Noetzli J, Arenson L, Delaloye R, Gärtner-Roer I, Gruber S, Isaksen K, Kneisel C, Krautblatter M, Phillips M (2010) Mountain permafrost: development and challenges of a young research field. J Glaciol 56(200):1043–1058

Haeni FP (1986) Application of seismic refraction methods in groundwater modeling studies in New England. Geophysics 51(2):236–249

Huss M, Bookhagen B, Huggel C, Jacobsen D, Bradley RS, Clague JJ, Vuille M, Buytaert W, Cayan DR, Greenwood J, Mark B, Milner A, Weingartner R, Winder M (2017) Toward mountains without permanent snow and ice. Earth's Future 5(May):418–435. https://doi.org/10.1002/eft2.207

Jacobsen D, Milner AM, Brown LE, Dangles O (2012) Biodiversity under threat in glacier-fed river systems. Nat Clim Chang 2(5): 361–364. https://doi.org/10.1038/nclimate1435

Johnson C, Lane J (2016) Statistical comparison of methods for estimating sediment thickness from Horizontal-to-Vertical Spectral Ratio (HVSR) seismic methods: an example from Tylerville, Connecticut, USA. In: Symposium on the Application of Geophysics to Engineering and Environmental Problems 2015. Society of Exploration Geophysicists, Tulsa, OK, pp 317–323

Jongmans D, Bievre G, Renalier F, Schwartz S, Beaurez N, Orengo Y (2009) Geophysical investigation of a large landslide in glaciolacustrine clays in the Trièves area (French Alps). Eng Geol 109(1):45–56

Juen I, Kaser G, Georges C (2007) Modelling observed and future runoff from a glacierized tropical catchment (Cordillera Blanca, Peru). Glob Planet Chang 59(1–4):37–48. https://doi.org/10.1016/j.gloplacha.2006.11.038

Kaser G (1999) A review of the modern fluctuations of tropical glaciers. Glob Planet Chang 22(1–4):93–103

Kaser G, Georges C (1999) On the mass balance of low latitude glaciers with particular consideration of the Peruvian Cordillera Blanca. Geogr Ann 81(4):643–651

Kaser G, Osmaston H (2002) Tropical glaciers. Cambridge University Press, Cambridge

Klimeš J (2017) Geomorphology and natural hazards of the selected glacial valleys, cordillera blanca, peru. Auc Geographica 47(2): 25–31. https://doi.org/10.14712/23361980.2015.14

Kneisel C (2004) New insights into mountain permafrost occurrence and characteristics in glacier forefields at high altitude through the application of 2D resistivity imaging. Permafr Periglac Process 15(3): 221–227

Kurtzman D, Baram S, Dahan O (2016) Soil-aquifer phenomena affecting groundwater under vertisols: a review. Hydrol Earth Syst Sci 20(1):1–12. https://doi.org/10.5194/hess-20-1-2016

Langston G, Bentley LR, Hayashi M, McClymont A, Pidlisecky A (2011) Internal structure and hydrological functions of an alpine proglacial moraine. Hydrol Process 25(19):2967–2982

Lavoie M, Paré D, Fenton N, Groot A, Taylor K (2005) Paludification and management of forested peatlands in Canada: a literature review. Environ Rev 13(2):21–50. https://doi.org/10.1139/A05-006

Lermo J, Chavez-Garcia FJ (1994) Are microtremors useful in site response evaluation? Bull Seismol Soc Am 84(5):1350–1364. https://doi.org/10.1306/080700710318

L'Heureux JS, Long M (2016) Correlations between shear wave velocity and geotechnical parameters in Norwegian clays. In: Proceedings of the 17th Nordic Geotechnical Meeting, Reykjavik, Iceland, May 2016

Loke MH (2000) A practical guide to 2-D and 3-D surveys. Electrical Imaging Surveys Environ Eng Studies 2000:8–10

López-Moreno JI, Valero-Garcés B, Mark B, Condom T, Revuelto J, Azorín-Molina C, Valero-Garces B, Moran-Tejeda E, Vicente-Serrano S, Zubieta R, Alejo-Cochachin J (2016) Hydrological and depositional processes associated with recent glacier recession in Yanamarey catchment, Cordillera Blanca (Peru). Sci Total Environ 579:272–282. https://doi.org/10.1016/j.scitotenv.2016.11.107

Maharaj L (2011) Investigating proglacial groundwater systems in the Quilcayhuanca and Yanamarey Pampas, Cordillera Blanca, Peru. MSc Thesis, McGill University, Montreal

Mark BG, Mckenzie JM (2007) Tracing increasing tropical Andean glacier melt with stable isotopes in water. Environ Sci Technol 41(20): 6955–6960. https://doi.org/10.1021/es071099d

Mark BG, Seltzer GO (2003) Tropical glacier meltwater contribution to stream discharge: a case study in the Cordillera Blanca, Peru. J Glaciol 49(165):271–281

Mark BG, McKenzie JM, Gómez J (2005) Hydrochemical evaluation of changing glacier meltwater contribution to stream discharge: Callejon de Huaylas, Peru. Hydrol Sci J 50(6):975–988. https://doi.org/10.1623/hysj.2005.50.6.975

Mark BG, Bury J, McKenzie JM, French A, Baraer M (2010) Climate change and tropical Andean glacier recession: evaluating hydrologic changes and livelihood vulnerability in the Cordillera Blanca, Peru. Ann Assoc Am Geogr 100(4):794–805. https://doi.org/10.1080/00045608.2010.497369

McClymont AF, Hayashi M, Bentley LR, Muir D, Ernst E (2010) Groundwater flow and storage within an alpine meadow-talus complex. Hydrol Earth Syst Sci 14:859–872. https://doi.org/10.5194/hess-14-859-2010

Michot D, Benderitter Y, Dorigny A, Nicoullaud B, King D, Tabbagh A (2003) Spatial and temporal monitoring of soil water content with an irrigated corn crop cover using surface electrical resistivity tomography. Water Resour Res 39(5):1138. https://doi.org/10.1029/2002WR001581

Moser TJ (1991) Shortest path calculation of seismic rays. Geophysics 56(1):59–67

Muir DL, Hayashi M, McClymont AF (2011) Hydrological storage and transmission characteristics of an alpine talus. Hydrol Process 25(19):2954–2966

Nakamura Y (1989) A method for dynamic characteristics estimation of subsurface using microtremor on the ground surface. Quarterly Report Railway Tech Res Inst 30(1):25–30

Nakicenovic N, Alcamo J, Grubler A, Riahi K, Roehrl RA, Rogner HH, Victor N (2000) Special report on emissions scenarios (SRES), a special report of working group III of the intergovernmental panel on climate change. Cambridge University Press, Cambridge

Oldenburg DW, Li Y (1999) Estimating depth of investigation in DC resistivity and IP surveys. Geophysics 64(2):403–416

Parsekian AD, Singha K, Minsley BJ, Holbrook WS, Slater L (2015) Multiscale geophysical imaging of the critical zone. Rev Geophys 53(1):1–26. https://doi.org/10.1002/2013RG000441.Received

Polk MH (2016) "They are drying out": social-ecological consequences of glacier recession on mountain peatlands in Huascarán National Park, Peru. PhD Thesis, Univ. of Texas, Austin, TX

Pollock DW (1989) Documentation of computer programs to compute and display pathlines using results from the US Geological Survey modular three-dimensional finite-difference ground-water flow model (No. 89-381). US Geological Survey

Pourrier J, Jourde H, Kinnard C, Gascoin S, Monnier S (2014) Glacier meltwater flow paths and storage in a geomorphologically complex glacial foreland: the case of the Tapado glacier, dry Andes of Chile (30 S). J Hydrol 519:1068-1083

Pouyaud B, Zapata M, Yerren J, Gomez J, Rosas G, Suarez W, Ribstein P (2005) On the future of the water resources from glacier melting in the Cordillera Blanca, Peru. Hydrol Sc J 50(6):999–1022. https://doi.org/10.1623/hysj.2005.50.6.999

Powers MH, Burton BL (2012) Measurement of near-surface seismic compressional wave velocities using refraction tomography at a proposed construction site on the Presidio of Monterey, California. US Geol Surv Open-File Rep 2012-1191

Racoviteanu AE, Arnaud Y, Williams MW, Ordoñez J (2008) Decadal changes in glacier parameters in the Cordillera Blanca, Peru, derived from remote sensing. J Glaciol 54(186):499–510. https://doi.org/10.3189/002214308785836922

Rodbell DT, Seltzer GO (2000) Rapid ice margin fluctuations during the younger Dryas in the tropical Andes. Quat Res 338:328–338. https://doi.org/10.1006/qres.2000.2177

Rodbell DT, Seltzer GO, Mark BG, Smith JA, Abbott MB (2008) Clastic sediment flux to tropical Andean lakes: records of glaciation and soil erosion. Quatern Sci Rev 27(15–16):1612–1626

Samouëlian A, Cousin I, Tabbagh A, Bruand A, Richard G (2005) Electrical resistivity survey in soil science: a review. Soil Tillage Res 83(2):173–193. https://doi.org/10.1016/j.still.2004.10.004

Sauret ESG, Beaujean J, Nguyen F, Wildemeersch S, Brouyere S (2015) Characterization of superficial deposits using electrical resistivity tomography (ERT) and horizontal-to-vertical spectral ratio (HVSR) geophysical methods: a case study. J Appl Geophys 121(November):140–148. https://doi.org/10.1016/j.jappgeo.2015.07.012

Schauwecker S, Rohrer M, Acuña D, Cochachin A, Dávila L, Frey H, Giraldez C, Gomez J, Huggel C, Jacques-Coper M, Loarte E, Salzmann N, Vuille M (2014) Climate trends and glacier retreat in the Cordillera Blanca, Peru, revisited. Glob Planet Chang 119:85–97. https://doi.org/10.1016/j.gloplacha.2014.05.005

Seht MIV, Wohlenberg J (1999) Microtremor measurements used to map thickness of soft sediments. Bull Seismol Soc Am 89(1):250–259

Somers L, Gordon R, McKenzie J, Lauta L, Wigmore O, Glose A, Glas R, Aubry-Wake C, Mark B, Baraer M, Condom T (2016) Quantifying groundwater-surface water interactions in a proglacial valley, Cordillera Blanca, Peru. Hydrol Process 2929(June):2915–2929. https://doi.org/10.1002/hyp.10912

Urrutia R, Vuille M (2009) Climate change projections for the tropical andes using a regional climate model: Temperature and precipitation simulations for the end of the 21st century. J Geophys Res Atmos 114(D2):D02108. https://doi.org/10.1029/2008JD011021

Vignoli G, Cassiani G, Rossi M, Deiana R, Boaga J, Fabbri P (2012) Geophysical characterization of a small pre-alpine catchment. J Appl Geophys 80:32–42

Vilímek V, Klimeš J, Červená L (2015) Glacier-related landforms and glacial lakes in Huascarán National Park, Peru. J Maps 5647(January):1–10. https://doi.org/10.1080/17445647.2014.1000985

Vuille M, Francou B, Wagnon P, Juen I, Kaser G, Mark BG, Bradley RS (2008) Climate change and tropical Andean glaciers: past, present and future. Earth-Sci Rev 89(3):79–96

Vuille M, Franquist E, Garreaud R, Sven W, Casimiro L, Cáceres B (2015) Impact of the global warming hiatus on Andean temperature. J Geophys Res Atmos. https://doi.org/10.1002/2015JD023126

Vuille M, Carey M, Huggel C, Buytaert W, Rabatel A, Jacobsen D, Soruco A, Villacis M, Yarleque C, Timm O, Condom T, Salzmann N, Sicart J (2018) Rapid decline of snow and ice in the tropical Andes–impacts, uncertainties and challenges ahead. Earth Sci Rev 176:195–213

Wigmore O, Mark B (2017) Monitoring tropical debris-covered glacier dynamics from high-resolution unmanned aerial vehicle photogrammetry, Cordillera Blanca, Peru. Cryosphere 11(6):2463

Winkler G, Wagner T, Pauritsch M, Birk S, Kellerer-Pirklbauer A, Benischke R, ... Hergarten S (2016) Identification and assessment of groundwater flow and storage components of the relict Schöneben Rock Glacier, Niedere Tauern Range, Eastern Alps (Austria). Hydrogeol J 24(4):937–953

Zelt CA, Smith RB (1992) Seismic traveltime inversion for 2-D crustal velocity structure. Geophys J Int 108(1):16–34